Palestinian Medical and Pharmaceutical Journal (PMPJ). 2023; 8(3): 343-366

# Homology Modeling of Human Indoleamine-Pyrrole 2,3-Dioxygenase-2 (hIDO2) and Virtual Screening Approaches to Identify Novel, Potent, and Selective HIDO2 Inhibitors

*Mohammed Qaoud*[1,*] *& Murat Şüküroğlu*[1]

[1] Department of Pharmaceutical Chemistry, Faculty of Pharmacy, Gazi University, Ankara, Turkey.

*Corresponding author: mqaud@daad-alumni.de

Received: (1/12/2022), Accepted: (12/1/2023)

## ABSTRACT

Indoleamine 2,3-dioxygenase 2 (IDO2) is a newly discovered target proposed to be a promising therapeutic modulator of various peripheral and central pathological states such as autoimmune disorders and immune escape diseases like cancer. The lack of potent hIDO2 inhibitors presents a high demand for discovering novel hIDO2 inhibition strategies to explore its indeed pathological role. We aim to develop novel, selective, and potent hIDO2 inhibitor candidates by building a new operative hIDO2 homology model and utilizing the computational structure/ligand-based methods. First, an IDO-focused library of hits besides a new library of candidates, which was self-designed based on the previously reported IDO2 inhibitors, was extracted and prepared, respectively, to be ready for the virtual screening procedure. Next, 14 potentially competent models were built, and the most promising models were selected for molecular docking simulations to search a group of potential candidates through their docking scores, ligand binding energies, and ligand-interaction patterns. Among the potential candidates, **Model 4** was the most competent model for high-throughput screening. The molecular docking results suggest that nine novel ligands might be promising candidates for the hIDO2 target. These candidates revealed ideal geometry and interaction patterns within the hIDO2 binding site compared to the reference compounds. Moreover, the candidates showed favorable ligand binding energies and exhibited druggability properties. These compounds could inspire further studies to discover advanced lead compounds for hIDO2 inhibition. Developing novel hIDO2 inhibitors to intervene in the pathological states that trigger autoimmune diseases or equally serious outcomes such as cancer could be significantly beneficial.

**Keywords:** Human Indoleamine-Dioxygenase-2, virtual screening, homology modeling, molecular docking studies, interaction patterns.

## INTRODUCTION

Tryptophan (Trp) is an essential amino acid largely metabolized through the kynurenine pathway. The kynurenine pathway drives various pathophysiological and physiological processes by producing biologically-active metabolites and depletion of local Trp concentration. The kynurenine pathway is in action in the periphery and central nervous systems. It controls various common and high-risk diseases such as cancer, cerebral malaria, neurological and neurodegenerative diseases, chronic inflammation, infectious diseases, allergic and autoimmune disorders, transplantation, and neuropathology (1, 2).

In the kynurenine pathway, the first reaction is the oxidative cleavage of the indole ring of tryptophan (Trp), converting Trp to N-formyl kynurenine. Trp is an essential amino acid, and its demand must be supplied from the diet; however, it is the least abundant of all dietary amino acids. The kynurenine pathway is the major consumer of the dietary Trp through converting it to numerous metabolites such as quinolinic acid (QA) as a neuroactive substrate, xanthurenic acid (XA), picolinic acid (PA), and anthranilic acid (AA). Furthermore, the kynurenine pathway is the main route for nicotinamide adenine dinucleotide ($NAD^+$) synthesis (3). The depletion of Trp triggers various physiological actions such as modulation of the immune responses; thus, it influences transplantation and the development of tolerance of tumors. In addition, the lack of Trp causes significant effects on cell proliferation by slowing down cell division, especially that of T-cells, and could be related to the proliferation of pathological microorganisms (4).

The kynurenine pathway could be catalyzed independently by three enzymes: indoleamine 2,3-dioxygenase 1 (IDO1), indoleamine 2,3-dioxygenase 2 (IDO2), and tryptophan 2,3-dioxygenase (TDO2). The IDO1 and TDO2 have been extensively studied, while the IDO2 paralog could be considered a newcomer to the field (3, 5). IDO1 and IDO2 are found in all mammals, and these isoforms are supposed to have arisen primarily through gene duplication. Other vertebrates, such as amphibians, birds, and fish, are likely to have just one type of IDO with a high amino acid sequence similarity to the mammalian IDO2. These observations assume that the ancestral IDO was more IDO2-like (6-8). Although three enzymes catalyze the kynurenine pathway, their biochemical characteristics and expression patterns are distinct, indicating the presence of unique biological roles for each enzyme. For instance, the expression pattern of IDO1 differs dramatically from its paralog IDO2. IDO2 is found in a limited number of tissues, such as the cerebral cortex and antigen-presenting cells (APCs) of the immune system, which includes dendritic cells (DCs) and B cells, and also in the kidney and liver.

On the other hand, IDO1 is expressed in much more diverse tissue types (9). Additionally, in the reproductive system of males, IDO2 is expressed in the tails of the spermatozoa; however, IDO1 and TDO2 are found in the apical and principal cells of the epidermis and the head of the spermatozoa, respectively (10). In a wide range of cell types, both expression level and activity of IDO1 isoform are stimulated in response to inflammatory stimuli and involved in manipulating responses to infection and inflammation (11, 12). For example, in endothelial cells, a high induction of IDO1 was observed during cerebral malaria; thus, the metabolite production level of the kynurenine pathway is increased (13, 14). It was noticed that blood pressure drops down in response to kynurenine pathway metabolites during sepsis and malaria (15). Moreover, studies on dendritic cells extracted from tumor-draining lymph nodes show that a high expression level of IDO1 is associated with a poor prognosis; this observed effect is proposed to be a result of suppressing the immune responses generated normally against the tumor (16, 17).

*Dextro*-1-methyl-tryptophan (D-1MT, Indoximod, NLG-8189), a well-known IDO1 inhibitor, is prescribed in cancer immunotherapy trials as an adjuvant to chemotherapeutic compounds such as paclitaxel (18-21). However, the *Levo*-1-methyl-tryptophan (L-1MT) displayed a higher IDO1 enzymatic inhibition potency than D-1MT, while D-1MT of the *Dextro*-type chirality displayed superior antitumor efficiency as a chemotherapeutic agent (22, 23). This set in a scientific debate about the physiological and pathological role of IDO1 enzyme, especially in cancer. This debate is further supported after discovering the IDO2 isoform and observing that the D-1MT has better IDO2 enzymatic inhibition potency than L-1MT (24, 25). Surprisingly, new reports confirmed the ability of IDO2 to modulate autoimmune diseases via acting on B cells as an immunomodulatory enzyme, which suggests that the action is different from its paralog IDO1. In multiple models of autoimmune inflammatory disorders, the newly found enzyme IDO2 works as a pro-inflammatory mediator of such pathological states as CHS (Contact hypersensitivity), RA (Rheumatoid arthritis), and SLE (Systemic lupus erythematosus). Recently, investigating the antitumor efficiency of epacadostat, a selective IDO1 inhibitor used in patients with metastatic or unresectable tumors, revealed disappointing results in phase III clinical trials (26). Observations that human pancreatic cancer cell lines have an IDO2 over-expression uphold the conception that the IDO2 isoform has a crucial role in promoting inflammation and tumor development which is distinct from its paralog IDO1 and could represent a new drug target in cancer immunotherapy, particularly as a co-therapeutic setting (27-29). Hence, the pathophysiological function of IDO2 is still unclear and needs to be understood via developing new selective IDO2 inhibitors that could have therapeutic potential in diverse pathological states, including tumorigenesis, inflammatory, and autoimmune diseases used alone or in combination with other antitumor agents or B-cell-depletion therapies. In addition, discovering IDO2 inhibitors could be valuable in determining the role of IDO2 in

tissues that exhibit constitutive expressions of IDO2, such as the reproductive system, kidney, and liver (30, 31).

The three enzymes hIDO1, hIDO2, and hTDO all have a prosthetic group of heme ($Fe^{+3}$), and for optimal enzymatic activity, the ferric group ($Fe^{+3}$) should be reduced to Ferrous ($Fe^{+2}$) (32-34). Thus, the IDO2 inhibitors prefer having at least one heteroatom (either oxygen or nitrogen) to coordinate with the heme iron. Concerning their amino acid sequences, hIDO1 and hIDO2 are homologous and share moderate overall amino acid sequence identity, which is about 43%, while TDO2 is not homologous to other IDO enzymes (7, 30).

A limited number of studies focus on the IDO2 paralog and mostly investigate the mouse type (with an amino acid sequence identity of 75% to hIDO2 and almost identical in the heme-binding pocket). One of the most recent studies presents a potent hIDO2 inhibitor with moderate selectivity developed through modifying a previously discovered hIDO1/hIDO2 dual inhibitor. The structure CPN- 22 (Figure 1-A) displayed for the first time a hIDO2 inhibition activity at the nanomolar level ($IC_{50}$ = 112 nM). Studying the anti-inflammatory effect of this newly discovered candidate showed a diminishing of inflammatory cytokines in both adjuvant arthritis (AA) in the rat model and collagen-induced arthritis (CIA) in the mice model (35). Another study aimed to identify mouse IDO2 inhibitors via performing a high throughput screening over a library of approved Food and Drug Administration (FDA) drugs like proton pump inhibitors, $Ca^{+2}$ channel blockers, and antifungals. As a result, the chemical structures of some candidates identified as selective mIDO2 inhibitors, such as miconazole, clotrimazole, lansoprazole, pantoprazole, and tenatoprazole are shown in (Figure-1 B-F). The most potent, selective, and promising candidate from the chosen classes was tenatoprazole with an $IC_{50}$ of 1.8 μM against mIDO2, while no activities were observed at 100 μM concentration against both mIDO1 and mTDO2 (36).

Here, we aimed to identify novel and selective hIDO2 inhibitors as a novel target which could be a new path for treating complex diseases such as cancer, neurodegenerative diseases, autoimmune disorders, and neuropathology. To enhance the screening efficiency, two libraries of candidates were applied; one is a focused IDO already prepared library, and the second is a self-designed library built by fragmenting the pre-identified IDO2 inhibitors and building a new library of small molecules. This was followed by examining the hIDO2 structure concerning the amino acid sequence and the 3D-structure of its binding pocket, building a hIDO2 homology model as the protein is yet to be crystallized, investigating the interaction patterns of previously discovered IDO2 inhibitors, and finally performing virtual screening and molecular docking studies to identify new potent and selective hIDO2 hits. In light of our findings, to our knowledge, we present one of the first studies to discuss valuable tools for hIDO2 inhibition and to guide and contribute to future efforts.

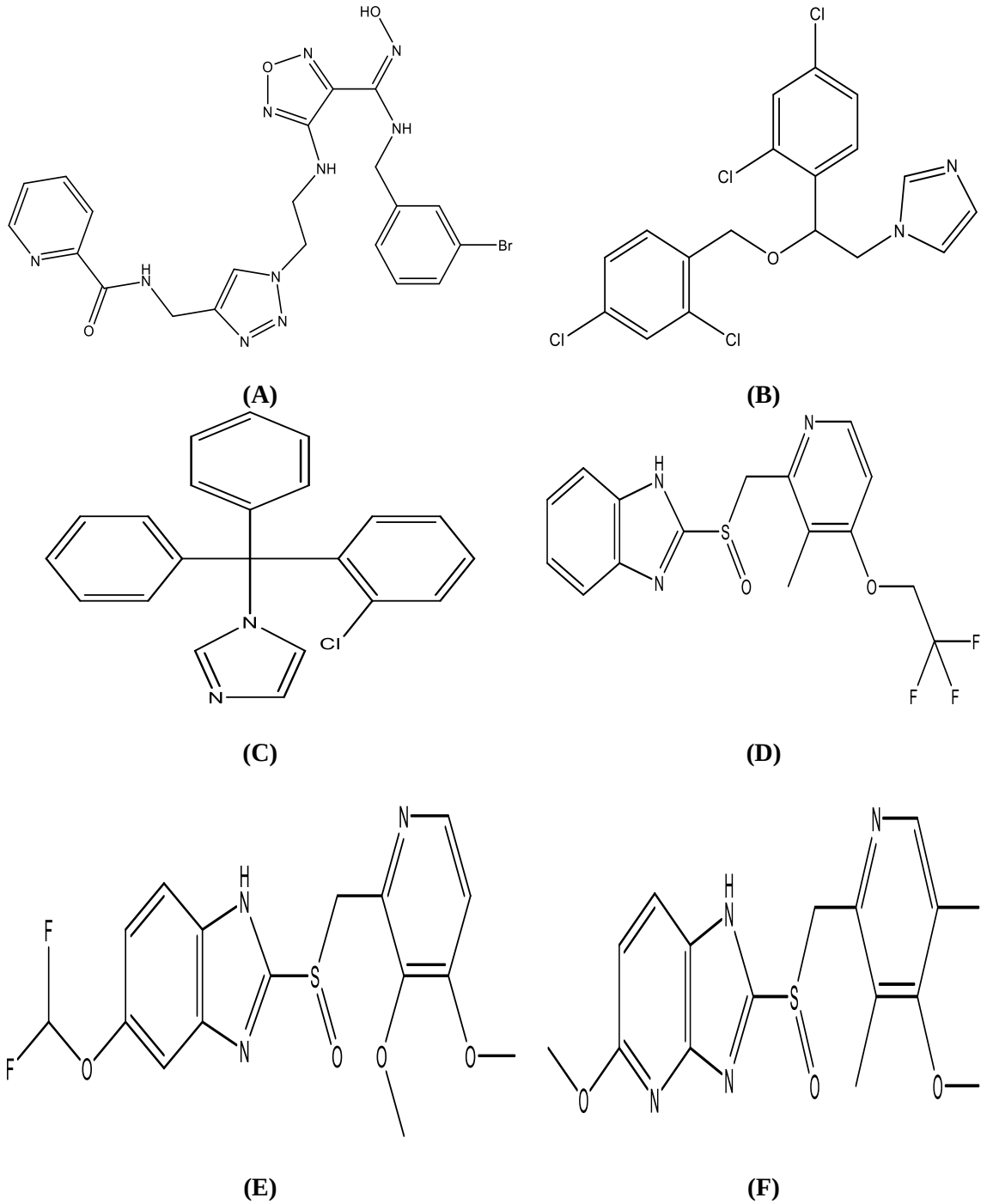


**Figure (1):** Chemical structures of previously discovered hIDO2 inhibitors**. (A)** CPN-22 **(B)** Miconazole **(C)** Clotrimazole, **(D)** lanzoprazole, **(E)** pantoprazole, **(F)** tenatoprazole.

## MATERIALS AND METHODS

### *General scheme of work*

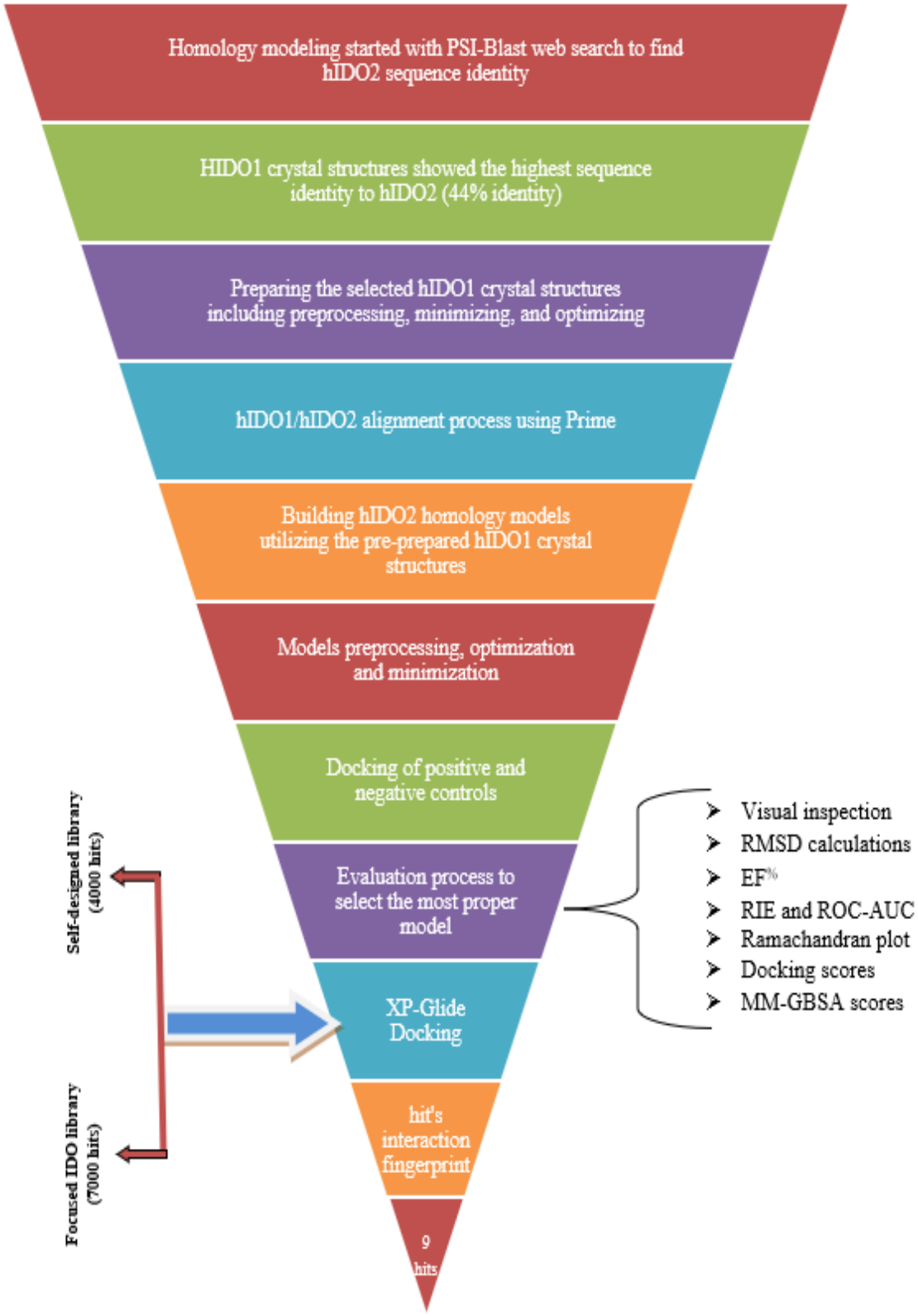

### *Building hIDO2 homology models*

To diminish the risk of getting false positive hits, two libraries of hits were applied, the 1st is an already prepared library called Indoleamine 2,3 Di-oxygenase-1 Focused Library, and the 2nd is a self-prepared library. The fir[st] library included around 7000 hits and was extracted from the website https://www.chemdiv.com/catalog/focused-and-targeted-libraries/indoleamine-2-3-dioxygenase-1-focused-library/ and directly uploaded to the maestro program and was ready for docking studies. The screening procedure of that library implicated data analysis step (clustering, isosteric morphing, pharmacophores extraction, and templates design), substructure searching according to that pharmacophore mode, and finally, applying a filtering procedure to get a final IDO-focused library of hits. A new library of hits was self-designed to improve the virtual screening efficiency and enhance the probability of getting potent and selective designs. The second new library of candidates was created based on the chemical structures of candidates reported as the most potent and selective IDO2 inhibitors by following the conditional design strategy and bioisosterism rules. The design strategy was based on merging and modifying the terminals and linkers of these candidates to achieve better geometry, interaction patterns, and occupying capacity within the binding site. Thus, the seco[nd] library of hits included about 4000 candidates were designed. So, we got a library of about 11,000 hits that will be used for the virtual screening studies (37, 38).

### *Ligand preparation*

The newly designed hits were prepared to utilize the Ligprep module integrated into maestro-Schrödinger 12.1. This process implicates the addition of hydrogen atoms and realizing the bond length, angles, stereochemistries, and ring conformations. Also, it includes generating the ionization states at target pH (7.4 ± 1.0), possible tautomers, low energy structures, and corrected chiralities of each ligand. Then, minimizing those preprocessed ligands at the force field OPLS-2005 using a default setting until getting an RMSD cut of 0.001 Å. The finally obtained minimized structures were then saved for molecular docking studies (39).

In our study, three programs and servers were applied to build homology models to select the most proper one:

1. *Swiss-Model server*

It is an easy and direct way to insert the hIDO2 amino acid sequence, followed by a blast search tool to find structure templates. The highest-ranked template was selected to build models of the hIDO2 protein structure (40). The amino acid sequence of hIDO2 had been obtained from the UniProt server as a blast file, and the UniProt code is Q6ZQW0 (I23O2_HUMAN).

2. *MPI Bioinformatics toolkit (HH-pred) server*

The process started with submitting the hIDO2 amino acid sequence and selecting PDB-mmCIF70_12_Aug as the structural/domain database. Then, the process involved analyzing the submitted sequence, predicting the sequence features, Query MSA generation, generating query A3M, and finally searching the profile HMM database. Then, the highest-ranked hitlist was used for building our homology model of hIDO2 (41).

3. *Maestro (version 12.1) Program (Prime-homology modeling)*

The homology model module (structure prediction wizard) integrated into the Maestro interface (Schrödinger 12.3) built twelve hIDO2 homology models using one or two hIDO1 templates. Many steps were followed to get highly reasonable and proper homology models (42):

*Selecting the proper crystal structure (templates):* The selection process started with applying the Basic Local Alignment Search Tool (PSI-BLAST) search module (blast.ncbi.nlm.nih.gov), integrated into the maestro program, using the target protein sequence (hIDO2) as the query sequence and PDB as the database. The top-ranked PDB codes that showed the best identity to hIDO2 were collected.

*Protein preparation*: The selected X-ray crystal structures of hIDO1 complexed with $Fe^{+2}$-porphyrin cofactor and different ligands were prepared with the Protein Preparation Wizard Workflow integrated into the Maestro module (Schrödinger 12.3, LLC). This process aimed to fix the crude crystal structure obtained via filling in missing loops using prime, verifying proper assignment of bonds, filling in missing side chains, deleting water molecules beyond 5 Å from the hit group, creating zero-order bonds to metals, adding hydrogens, creating disulfide bonds, and as final minimizing the protein structure and bonds (43). These prepared hIDO1 crystal structures were utilized as templates for building.

*Alignment using the prime STA method*

*Energy-based building model*

***Molecular docking studies***

Molecular docking studies usually follow a general procedure that starts with preparing ligands, selecting and preparing appropriate protein structures, and grid generation. This is followed by examining ligand-receptor interaction patterns and analyzing docking poses and scores. Ligand and protein preparation steps were applied using the LigPrep and Protein preparation Wizard modules integrated into the maestro program, as explained before.

Regarding receptor grid generation, the receptor grids of the hIDO1 crystal structures and the newly built hIDO2 homology models were generated using the Receptor Grid Generation module integrated into the Maestro interface. The grid boxes were defined as a 20 × 20 × 20 Å space region centered at the original ligand of the complex structures. In addition, one metal coordination was introduced into heme during grid box generation. For the other parameters, the default values were assigned. The extra-precision mode of the Glide module (Glide score XP) integrated into the Maestro (Schrödinger 12.3) was utilized (44). After the molecular docking studies were completed, the Protein-Ligand Interaction Profiler (PLIP) server was applied to evaluate the binding modes (45).

***Evaluating the newly built homology models***

The previously reported hIDO2 selective inhibitors (Tenatoprazole and CPN-22) were considered reference candidates (36, 46). These previously published inhibitors were preprocessed besides our newly prepared hits library and were docked into the binding site of both hIDO1and hIDO2-homology model using Glide (version 12.3, Schrödinger, LLC, New York, NY, 2022) in extra precision (XP) mode.

In order to select the most reasonable hIDO1 crystal structure and hIDO2 homology model, many strategies were followed, including:

*Visual inspection*

- The 3D structures were compared to the literature, and the absence of any cracks or missing regions was checked.
- The interaction patterns and geometry of positive controls were compared to published data in the literature.
- The proper amino acid alignment of hIDO1 and hIDO2 models in their 3D structures upon superposition was checked. The position of every amino acid was checked and ensured that it was truly superposed.

*Root-Mean-Square Deviation (RMSD)*

Calculating RMSD is the simplest method for evaluating the reliability of the 3D structures within their experimental counterpart.

The built 3D-homology models were subjected to two RMSD calculations.

*Ligand / Ligand RMSD (called RMSD of native docking):* The ligand binding to the hIDO1 template was prepared using the LigPrep module. Then, this native ligand was docked to the homology model, which was built utilizing that crystal structure template. Those docked ligands were superposed on their crystal state, and RMSD was calculated.

*Protein / Protein RMSD:* The hIDO2 3D-homology models' backbones were superposed on the hIDO1 crystal protein backbone template, and RMSD was calculated.

Regarding the hIDO1 crystal structures, only the RMSD of native docking (L/L RMSD) was calculated.

*Enrichment Factor ($EF^{x\%}$):* The EF

measures the enrichment of active compounds in a molecular dataset given a specific percentage of that dataset (threshold). The EF is the ratio between ligands (hits) found using a certain threshold *x* % ($Hits^{x\%}$). The number of compounds at that threshold $N^{x\%}$ normalized by the ratio between the hits in the entire dataset ($Hits^{100\%}$) and the total number of compounds $N^{100\%}$. EF is used to evaluate the ability of a virtual screening model to identify actives from in-actives, which was defined as Equation (1).

$$EF = \frac{Hits\ set}{n} / \frac{Hits\ all}{N} \qquad \text{(eq. 1)}$$

**Hits** set is the number of actives in the selected subset ***n*** of the ranked database, and **Hits all** is the total number of actives in the database of ***N*** compounds (47).

*Receiver Operating Characteristics - Area Under the Curve (ROC-AUC) and robustinitial enhancement (RIE)*

The ROC curve indicates the ability of a program to distinguish between ligands and decoys (48).

*Ramachandran Plot*

Ramachandran plots serve as an indirect verification tool of the stereochemistry and geometry ofthe complex by establishing that none of the geometries are in the forbidden electrostatically unfavored regions of the plot. A good quality model would be expected to have over 90% of residues in the most favored regions (49).

*XP-Glide Docking Studies*

The prepared enzyme structures and homology models were evaluated based on their ability to properly rank the potent candidates with higher docking scores compared to low potent candidates that are supposed to show low docking scores.

*MM-GBSA*

The capability of hIDO1 crystal structures and the newly built homology models to rank the potent candidates firstly, in contrast to non-potent, concerning the binding affinity using the prime Molecular mechanics – Generalized Born Model and Solvent accessibility (Prime MM-GBSA) model integrated into the Maestro-Schrödinger 12.3 program. The MM-GBSA model estimates the ligand binding energies and the ligand strain energies of the docked molecules within the binding pocket. The Prime MM-GBSA model worked at the OPLS-2005 force field and VSGB solvent model (The VSGB 2.0 Model, 2017). Thus, the total free energy of ligand-receptor binding was calculated using the resulting Glide pose viewer file of the docked ligands. Upon binding, the following Equation is applied to calculate the changes in free energy:

ΔG bind = G complex – (G protein + G ligand) ----------Eq.1

Where ΔG bind is the ligand-binding energy, G complex, G-protein, and Gligand are the minimized energies of protein-ligand complex, unbound protein, and unbound ligand, respectively (50).

***Selecting hIDO1 crystal structures***

Aiming to estimate the selectivity of our proposed hits over hIDO1 paralog, there is a demand to study their interaction patterns within hIDO1 via applying molecular docking and MM-GBSA studies. To select a proper hIDO1 crystal structure, evaluating parameters such as RMSD, ROC-AUC, RIE, and EF calculations were applied.

***Molecular docking studies and selection criteria of promising potent hIDO2 hits***

Obtaining a proper hDO2 homology model was followed by subjecting the newly built library of hits to molecular docking and binding affinity studies. The library of hits was docked to the selected model. To select the most promised hits that are expected to work as a new, novel, and selective hIDO2 inhibitor, well-established criteria were followed and based on the following:

- Top 0.5% ranked XP-docking score.
- Top 0.5% ranked MM-GBSA score.
- The ability to perform π-π stacking or hydrophobic with deeply embedded residues like F-180 and ILE-181 indicates that the hit penetrates deeply to the hIDO2 binding site.
- Perform a short and strong coordination bond with $Fe^{+2}$-porphyrin.
- They form superior hydrogen bonds

and hydrophobic and polar interactions.

- Occupy the binding pocket optimally.
- Optimally ADME-T parameters.
- Have a good selectivity over the hIDO1 paralog.

These summarized criteria are superior to that observed in CPN-22 and tenatoprazole.

### *Drug likeness analysis*

In order to assess the druggability of our finally selected candidates, the drug-likeness was assessed by calculating a set of descriptors referred to the absorption, distribution, metabolism, excretion, and toxicity (ADME-T). The QikProp module integrated into the maestro Schrödinger suite (Schrödinger Release 2022-3) was used to estimate the ADME-T descriptors. It is an easy-to-use, quick, and accurate module (51, 52).

## RESULTS

### *Building of hits library*

To build the 2nd (self-designed) library, The CPN-22, and the proton pump inhibitor tenatoprazole showed the best potency and selectivity toward IDO2 enzyme over the IDO1 paralog (35, 36). Fragmenting these ideal candidates and trying to merge or modify these parts to various bioisosteric analogs, which could simulate these replaced parts, resulted in designing a new library of about 4000 hits. These newly designed hits were drawn and subjected beside the 1st (focused IDO library) into maestro-Schrödinger 12.3 to be prepared using the LigPrep module.

### *Building of homology models*

*Swiss-Model server*

Using the Swiss-Model server, a hIDO2-homology model (**model 1**) was built based on the hIDO1 crystal structure (PDB code 7E0U.1.A, X-ray resolution = 2.28 Å), Sequence identity = 45.31%, coverage range 30-416 a.a. (ratio = 0.91), QMean = 0.76, Ramachandran favored = 95.6%. The heme-porphyrin and the ligand were added by superposing the newly built homology model on the crystal structure of hIDO1-7E0U. The heme-porphyrin structure connected covalently to HIS-360, and the binding site was checked and defined precisely.

*MPI Bioinformatics toolkit (HH-pred) server*

The homology **model, 2 of the hIDO2 enzyme,** was built using the HH-pred based on the top-ranked hIDO1 crystal structure (PDB code 6E43-B (X-ray resolution = 1.7 Å), Identities 44%, Similarity: 0.815, probability 100, E value = 6.8e-73, Score: 567.07, Aligned cols: 387, Template Neff: 8.8. The 3-D model structure was gotten as PDB file then once superposed to its template, the ligand, and heme-porphyrin were added to the model. The heme-porphyrin structure formed a covalent bond to HIS-360, and the ligand was identified precisely within the binding site.

*Maestro Program version 12.1 (Prime-homology modeling)*

As the maestro program is a comprehensive and advanced tool to perform bioinformatics studies, including homology modeling, the modeling process could be controlled at many stages, from selecting and preparing the crystal templates to the final step of building a homology model.

*Selecting the Proper Crystal Structures (templates)*

As a result of applying PSI-BLAST search on the target protein sequence of hIDO2 as a query sequence and PDB as a database, the top-ranked PDB protein codes showed the highest amino acid identity (44%) to hIDO2 were collected. Those noted PDB codes are summarized in (Table 1) including their X-ray resolution, missing amino acid, and crystallized ligands. All crystal structures were found with missing amino acids of chain loop structure (generally at amino acid 361-379), usually lost during crystallization. The selected structures have excellent X-ray resolutions (less than 3 Å) except 2D0U, with a resolution equal to 3.4 Å.

After that, these hIDO1 templates were prepared, optimized, minimized then utilized separately for homology modeling. As a result, twelve hIDO2 homology models (**models 3 – 14**) were built.

All the newly built models were prepared, optimized, and minimized to be ready for docking and evaluation studies.

**Table (1)**: PDB codes of hIDO1, resolution, missing parts, and ligands.

| PDB code | X-ray resolution (Å) | Missing a.a. | ligand |
|---|---|---|---|
| 2D0T | 2.3 | 361-379 | 4-phenyl imidazole |
| 2D0U | 3.4 | 361-379 | cyanide |
| 7E0S | 2.7 | 363-380 | (1R,2S)-2-(((6-Bromo-1H-indazol-4 yl)amino)methyl) cyclohexane-1-ol |
| 7E0Q | 2.46 | 361-381 | (1S,2R)-2-(((6-Bromo-1H-indazol-4-yl)amino) methyl) cyclohexane-1-ol |
| 7E0U | 2.27 | 363-373 | 6-Bromo-N-(((1S,2S)-2-chlorocyclohexyl)methyl)- 1H-indazol-4-amine (39) |
| 7E0T | 2.1 | 361-378 | (1R,2S)-2-(((5-Bromo-1H-indazol-4-yl)amino) methyl) Cyclohexan-1-ol |
| 4U74 | 2.31 | 363-379 | 4-phenyl imidazole |
| 6E43 | 1.71 | | BMS-978587 |

***Evaluation tools***

In order to choose the most reasonable hIDO2 homology models, which could be used confidently in screening studies, all 14 models of hIDO2 were subjected to the following discriminatory evaluation tools:

*Amino acid superposition in 3-D structure*

Upon superposing the newly built homology models on their templates, the amino acids superposition of the hIDO2 homology model and the hIDO1 crystal structure template was checked. It was the first time to detail the opposing amino acids observed in 3-D structures. As shown in (Table S1) (supplementary materials), the differences between paralogs hIDO1 and hIDO2 concerning the binding position of $Fe^{+2}$-porphyrin structure and amino acids sequencing within the binding pocket and entrance gate during the 3-D superposition state are summarized, and the differences are highlighted. As observed, the $Fe^{+2}$-porphyrin cofactor of both paralogs binds to HIS amino acid but at a different position. The cofactor binds covalently to HIS-360 in hIDO2 but to HIS-246 in hIDO1 paralog. Checking the amino acids superposition revealed that the seven amino acids HIS-143, LEU-146, ILE-181, TYR-184, SER-277, LEU-368, and PRO-380, identified within the hIDO2 binding pocket, are replaced with TYR-126, CYS-129, PHE-164, SER-167, ALA-260, ILE-354, and GLU-364 in hIDO1, respectively. Concerning the pocket entrance, the two amino acids MET-234 and Val-400 in hIDO2 are replaced with ILE-217 and LEU-384 in hIDO1, respectively. Other amino acids identified within the binding pocket and entrance are found as identical types. All homology models showed similar superposition results, which indicate the high correlation between them, so further evaluating tools were applied to select the best proper one.

*Root-Mean-Square Deviation calculations*

To evaluate our 14 newly built homology models, both L/L RMSD and P/P RMSD were calculated. The calculated RMSD value refers to the distance average between all the atoms in two 3-D structures once superposed. It is a discriminative indicator that emphasizes the proper building process of homology models. Optimally, the P/P RMSD value should not exceed 2 Å to be applicable for another evaluation process; however, minimal perturbations in a loop between domains can result in a misleading high RMSD. Also, Getting an L/L RMSD value lower than 2 indicates that the molecular docking procedure works well (53). As summarized in (Table 2), **model 4,** which was built using the two templates 2D0T/2D0U, showed the best and ideal L/L and P/P RMSD values (less than 2) as a result of superposing **model 4 (**protein backbone +

ligand) on the both 2D0T and 2D0U. (Figures 2-A and B) show the 3-D structure superposition of **model 4** over the 2D0T backbone and ligand, respectively. It showed high 3-D structure fitting reflected that recorded low RMSD values. The amino acid sequence alignment of hIDO2 on 2D0T and 2D0U using Prime STA is shown in (Figure 2-C).

**Model 4**, as an ideal one, was selected to be subjected to a different evaluation process to ensure that it could be used confidently. Models 1, 3, and 5, which showed semi-ideal RMSD values due to little deviations in some regions, were also processed for the other evaluation parameters to get further supportive data.

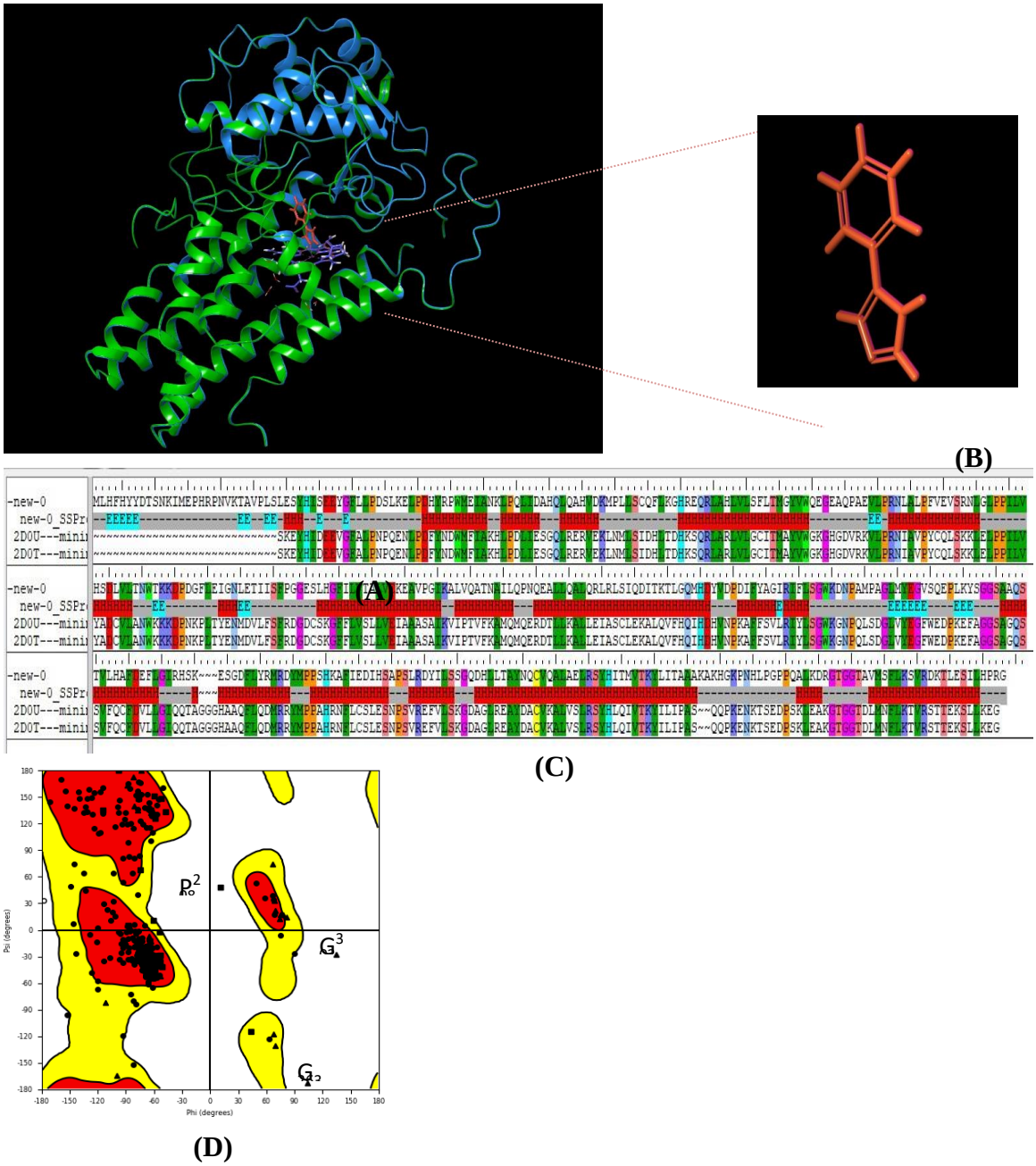


**Figure (2): (A)** protein backbone superposition of hIDO2 (model 4, green ribbon) on hIDO1 (PDB ID: 2D0T-A, blue ribbon). **(B)** Ligand Superposition between the docked pose of phenyl imidazole within hIDO2 model 4 (orange ribbon) and the native crystallized pose of hIDO1 (PDB ID: 2D0T-A, purple ribbon). **(C)** Prime STA alignment sequence of hIDO2 model 4 on the hIDO1 proteins (PDB ID: 2D0T and 2D0U). The red color indicates the presence of un-similarity in amino acid residues. **(D)** Ramachandran plot analysis of hIDO2-homology models 4. The Ramachandran plot allows φ/ψ distributions for homology models as determined in the Maestro program. Residues in the favored regions are located in the orange region, while residues in the allowed regions are in the yellow region. The outliers are proline 208, Glycine 303, and Glycine 263.

**Table (2):** The RMSD, enrichment factors, AUC-ROC, and RIE calculations of the newly built hIDO2-homology models using different programs.

| | Program | Number | hIDO1 PDB codes used | Enrichment calculation | | | | | | | Ligand superposition (RMSD) | | Protein superposition (RMSD) | |
|---|---|---|---|---|---|---|---|---|---|---|---|---|---|---|
| | | | | AUC-ROC | RIE | EF 1% | EF 2% | EF 5% | EF 10% | EF 20% | | | | |
| HIDO2 homology models | Swiss model | 1 | 7E0U | 0.81 | 4.92 | 14 | 7.2 | 5.2 | 4.3 | 2.1 | 7E0U: 1.15 | | 7E0U: 5.52 | |
| | HH-Pred | 2 | 6E43-D | - | - | - | - | - | - | - | - | | 6E43: 7.69 | |
| | Maestro program | 3 | 7E0T / 2D0T | 0.79 | 3.2 | 0 | 0 | 1 | 3 | 4 | 2D0T: 0.129 | 7E0T: 0.372 | 7E0T: 6 | 2D0T 3.1 |
| | | 4 | 2D0T / 2D0U | 0.8 | 6.13 | 29 | 14 | 5.8 | 4.3 | 2.1 | 2D0T: 0.139 | 2D0U: 0.24 | 2D0T: 1.6 | 2D0U: 1.9 |
| | | 5 | 7E0T / 7E0S | 0.82 | 4.53 | 14 | 7.2 | 5.8 | 2.8 | 2.9 | 7E0T: 0.74 | 7E0S: 1.04 | 7E0T: 2.8 | 7E0S: 4 |
| | | 6 | 7E0T / 6E43 | - | - | - | - | - | - | - | 7E0T: - | 6E43: - | 7E0T: 7.72 | 6E43: 2.83 |
| | | 7 | 7E0T / 4U74 | | | | | | | | 7E0T: 0.88 | 4U74: 0.32 | 7E0T: 3.22 | 4U74: 2.82 |
| | | 8 | 2D0T | - | - | - | - | - | - | - | 2D0T: 0.15 | | 2D0T: 2.84 | |
| | | 9 | 2D0U | - | - | - | - | - | - | - | - | | 2D0U: 2.83 | |
| | | 10 | 7E0T | - | - | - | - | - | - | - | 7E0T: 0.82 | | 7E0T: 2.82 | |
| | | 11 | 7E0Q | - | - | - | - | - | - | - | 7E0Q: 0.82 | | 7E0Q: 3.13 | |
| | | 12 | 7E0S / 2D0T | - | - | - | - | - | - | - | 7E0S: 1.17 | 2D0T: 0.14 | 7E0S: 3.41 | 2D0T: 2.84 |
| | | 13 | 7E0U / 2D0U | | | | | | | | 7E0U: 0.033 | 2D0U: 0.71 | 7E0U: 2.83 | 2D0U: 3.23 |
| | | 14 | 4U74 / 2D0T | - | - | - | - | - | - | - | 4U74: 0.21 | 2D0T: 0.20 | 4U74: 2.82 | 2D0T: 3.29 |

*Enrichment factor (EF $^{\%}$)*

The EF is an effective parameter applied to assess the power of the prepared protein structures to distinguish the active candidates from in-actives. Here, the homology **models 1, 3, 4,** and **5** were subjected to the Enrichment factor (EF $^{\%}$) tool at 1, 2, 5, 10, and 20. The EF$^{\%}$ values were calculated and summarized in (Table 2). The EF$^{20\%}$ presents the late-stage enrichment, while the EF$^{1\%}$ presents the early-stage enrichment. Regarding the tested hIDO2 homology models, **model 4** showed superior early-stage enrichments with EF$^{1\%}$ and EF$^{2\%}$ values equal to 29 and 14, respectively. This means that within the top 1% and 2% of the docking ranked database, 29 % and 14 % of the known ligands can be found, respectively. Within the moderate and later stages of enrichments (EF$^{5,\ 10,\ \text{and}\ 20\%}$), **models 1**, **4**, and **5** showed similar enrichment efficiency with less than 6. **Models 1** and **5** revealed similar EF at the early stage enrichment (EF$^{1\%}$ and EF$^{2\%}$) with EF equal to 14 and 7, respectively. **Model 3** was reported with poor enrichment and showed 0 enrichments at the early stages.

*Receiver Operating Characteristics - Area Under the Curve (ROC-AUC) and robustinitial enhancement (RIE)*

The ROC-AUC parameter is utilized to estimate the capacity of a method. It evaluates the ability of protein structure to differentiate between decoys and ligands and could be obtained from the ROC curves. Observing a ROC-AUC value closer to 1 and a higher RIE value indicates that the method has a better predictive ability than a random one (54). As summarized in (Table 2), **model 4** showed ideal ROC-AUC and RIE values equaled 0.8 and 6.13, respectively. **Models** 1, 3, and 5 showed similar ROC-AUC values but with lower RIE values, which indicates that **model 4** is still the proper one over the others.

The Ramachandran Plot analysis

Analysis of **model 4**, as shown in (Figure 2-D), regarding the Ramachandran plot, revealed that only three amino acids (proline 208, Glycine 303, and Glycine 263) were found outliers which indicates the propriety of **model 4,** while other models showed weak indications.

Binding Site Geometry and Enveloped Residues

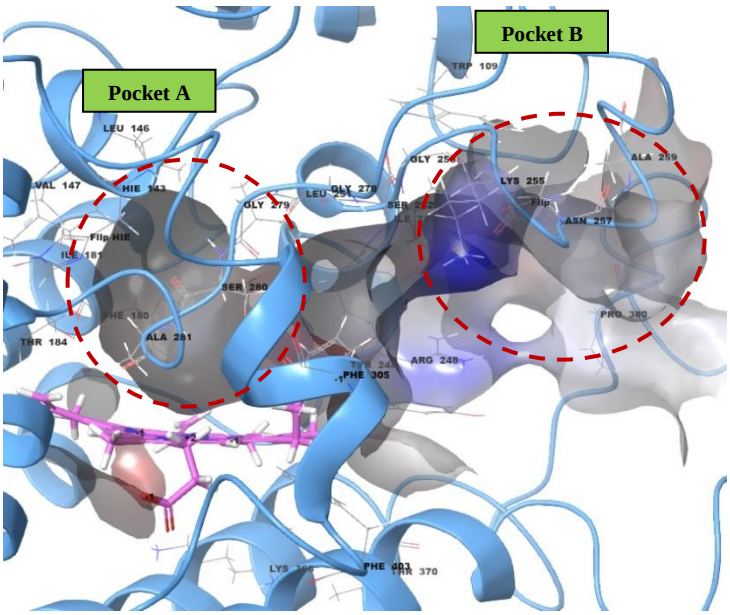
Pocket A
Pocket B
TRP 109
LEU 146
VAL 147
HIE 143
GLY 279
LEU 251
GLY 254
LYS 255
ALA 259
ASN 257
Flip HIE
ILE 181
SER 280
PHE 180
THR 184
ALA 281
ARG 248
PHE 305
PRO 380
PHE 403
THR 370

**(A)**

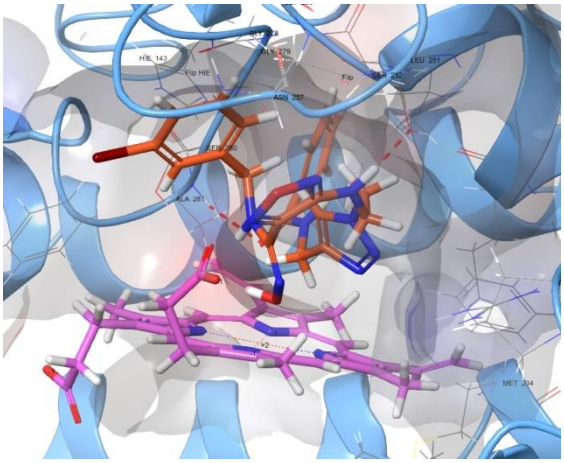

**(B)**

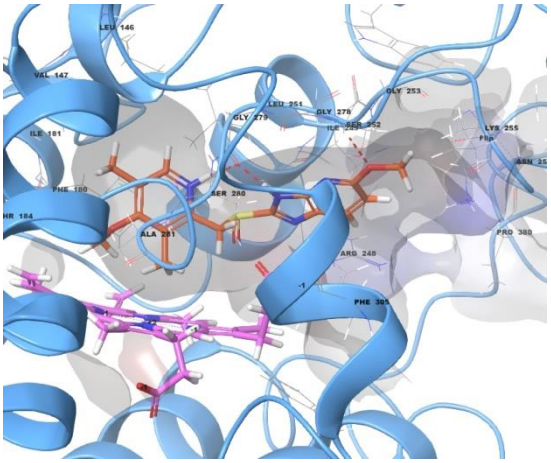

**(C)**

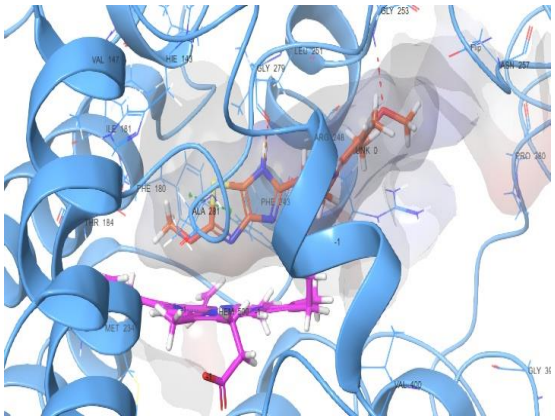

**(D)**

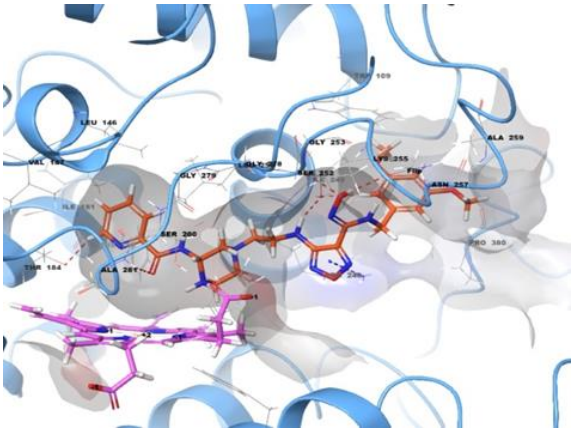

**(E)**

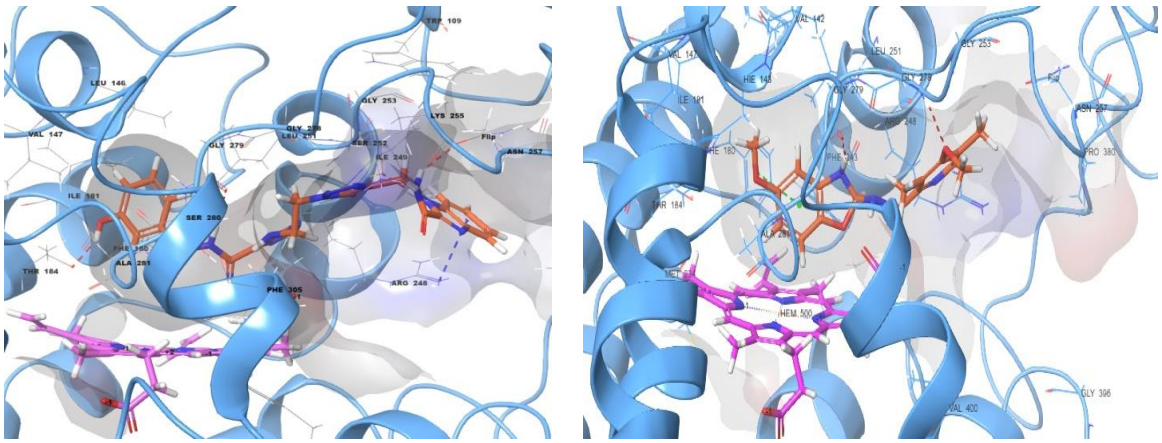

**(F)** **(G)**

**Figure (3): (A)** 3D-geometry of hIDO2 binding site displaying pocket A, B, linker, and solvent accessible region. Docking simulation of **(B)** CPN-22, **(C)** tenatoprazole, **(D)** A1-compound, **(E)** A3-compound **(F)** A4-compound, and **(G)** A7-compound within the binding pocket of hIDO2 homology model (based on 2D0T/2D0U). The active site is a 3D gray electrostatic surface (transparency 80%). Ligands are shown as stick structures-orange color. Red dashes represent hydrogen bonds; π-π stacking in green dash lines. Blue dash lines indicate the presence of the Pi-cationic bond.

As shown in (Figure 3-A), the binding site identified within **model 4** includes two main pockets, pocket A and pocket B. pocket A locates directly over the $Fe^{+2}$-porphyrin structure and is enveloped by such residues like L-146, H-143, and F-180, I-181, T-184. Pocket B is displayed as an elongated pocket, right to pocket A, and involves residues like K-255, N-257, G-278, and R-248. A linker-like groove connects the two pockets. Additionally, there is a solvent-accessible region that directly exists below pocket B. Those observed regions, geometries, and residues' positions are identical to those previously reported in the literature (35, 36).

*Molecular Docking Studies and MM-GBSA*

To evaluate the ability of homology **model 4** to hold the approved potent and selective hIDO2 properly, besides assessing the reliability of their binding interactions, geometry, docking scores, and binding energy within the binding pocket, molecular docking and MM-GPSA studies were applied. The calculated docking scores and ΔG binding energy of CPN-22 and tenatoprazole are summarized in (Table 3). CPN-22, the most potent hIOD2 previously found, showed docking score and binding energy equal to -7.5 and -80.24, respectively, which are higher than that observed for tenatoprazole (docking score = -6.6, ΔG binding energy = -75.26). Additionally, the binding geometry and interaction pattern of both compounds within the hIDO2 binding site is shown in (Figures 3-B and C) and found to be similar to that recorded in the literature. Both structures are characterized by forming short and advanced binding interactions with the $Fe^{+2}$-porphyrin, a crucial interaction for potency, besides many other favored hydrogen bonds and hydrophobic interactions with the surrounding residues. The 3D-docking simulations show a superior fitting of CPN-22 compared to tenatoprazole, consistent with the observed XP-glide docking score and ΔG-binding affinity. The observed ideal and advanced binding patterns and the ability to rank these selective ligands properly emphasize the reliability of **model 4**. Thus, it is a confident model and could be applied for our final screening.

**Table (3):** The XP- Glide docking scores, calculated binding energy (ΔG), and interaction patterns of the selected hits and positive control ligands:

| code | $Fe^{+2}$-porphyrin (A°) | H. Bs | π-π stacking | HPHO interactions | π-Cation interaction | Halogen bond | Docking score | MM-GBSA (ΔG) | hIDO1 | |
|---|---|---|---|---|---|---|---|---|---|---|
| | | | | | | | | | Docking score | MM-GBSA (ΔG) |
| A1 | 2.73 | G-253, G-279 | F-180 | L-146, F-180, R-248, L-251 | | | -8.32 | -85.30 | -4.94 | -55.12 |
| A2 | 1.68 | G-279, A-281 | | | | | -8.16 | -82.21 | -6.65 | -62.52 |
| A3 | 2.03 | R-248, S-252, G-253, N-257, A-259, G-279, A-281 | | L-146, V-147, F-180, I-181, L-251 | | | -9.24 | -105.91 | -8.03 | -60.79 |
| A4 | 2.14 | T-184, S-252, N-257, G-278, G-279 | | L-146, V-147, F-180, I-181, I-249, L-251, P-380 | R-248 | | -9.20 | -89.22 | -9.08 | -58.69 |
| A5 | 1.88 | G-253, G-279 | | F-180, A-281 | | | -7.1 | -73.78 | -4.6 | -50.45 |
| A6 | 2.19 | G-279 | | V-147, F-180, I-181, T-184, F-243, R-248, A-181 | | | -7.38 | -76.65 | -6.46 | -57.14 |
| A7 | 2.01 | G-253, G-279 | F-180 | A-281 | | | -8.05 | -79.15 | -7.51 | -66.54 |
| A8 | 3.75 | G-278 | F-180 | L-251, F-305 | | T-184 | -7.9 | -80.25 | -4.62 | -58.96 |
| A9 | 4.67 | R-248, L-251, S-252, G-278, A-281 | | F-180, L-251, F-305 | | | -7.5 | -78.19 | -5.20 | -59.85 |
| CPN-22 | 1.4 | S-252, G-279, A-281 | | V-147, F-180, I-181, L-252 | | | -7.58 | -80.24 | -7.01 | -49.65 |
| Tenatoprazole | 6.52 | G-253, G-278, G-279 | | V-147, F-180, T-184, A-281 | | | -6.60 | -75.26 | -4.025 | -64.43 |

**$Fe^{+2}$-porphyrin (Å)**: bond distance to $Fe^{+2}$ structure. **H. Bs:** hydrogen bonds. **π-π stacking**: pi-pi stacking bonds. **HPHO interactions**: hydrophobic interactions. **π-Cation interaction**: pi-cation interactions.

### *Selecting the hIDO1 crystal structure*

As shown in (Table 4), evaluating three PDB structures referred to the hIDO1 enzyme resulted in the PDB ID: 2D0T displaying the highest EF values at both primary stages, EF1%, and EF2%, equaled 17 and 8.4, respectively. Also, it showed that the lowest RMSD protein backbone equaled 0.075 and the optimum of both ROC-AUC and RIE values. Thus, the 2D0T backbone was selected to apply for the molecular docking and hits selectivity studies.

**Table (4):** Results of enrichment and RMSD calculations of hIDO1 crystals.

| PDB codes | AUC-ROC | RIE | EF 1% | EF 2% | EF 5% | EF 10% | EF 20% | Ligand superposition(RMSD) |
|---|---|---|---|---|---|---|---|---|
| **2D0T** | 0.74 | 3.09 | 17 | 8.4 | 3.4 | 1.7 | 0.83 | 0.075 |
| **7E0T** | 0.81 | 3.41 | 0 | 0 | 3.4 | 3.3 | 2.5 | 0.59 |
| **4U74** | 0.76 | 2.67 | 0 | 0 | 8.4 | 3.4 | 1.7 | 0.48 |

### *The finally selected hits*

The chemical structures of the finally selected hits are summarized in (Figure 4)**.** The docking scores, calculated binding energy (ΔG), and interaction patterns of the selected hits besides the positive control ligands (CPN-22 and tenatoprazole) are summarized in (Table 3). The 3D-docking simulations of comp. **As representative hits, A1, A3, A4, and A7** are shown in (Figure 3-D, E, F, and G)**,** respectively. As observed, all the selected hits showed superior XP-glide docking scores and ΔG-binding affinity besides exhibiting advanced interaction patterns and geometries compared to both positive controls (CPN-22 and tenatoprazole). In addition to that fruitful and advanced hydrogen bonds, hydrophobic interactions, and shorter coordination bonds to $Fe^{+2}$-porphyrin, hits like **A1**, **A4**, **A7**, and **A8** show special interactions that are supposed to play a key role in boosting docking scores and binding affinities such as π-π stacking and π-cationic interactions that did not be observed in the positive controls.

Additionally, as shown in the 3-D docking simulation, the binding site is much optimally occupied and filled by our newly discovered hits. All the selected hits are novel structures and predicted to have superior potency and selectivity over the previously tested ones. On the other hand, those ideal behaviors observed within the hIDO2 binding site contrast with that observed within the hIDO1 binding site. As summarized in (Table 3), they showed lower docking scores and ΔG binding energies as a result of that less optimal binding patterns and interactions within hIDO1.

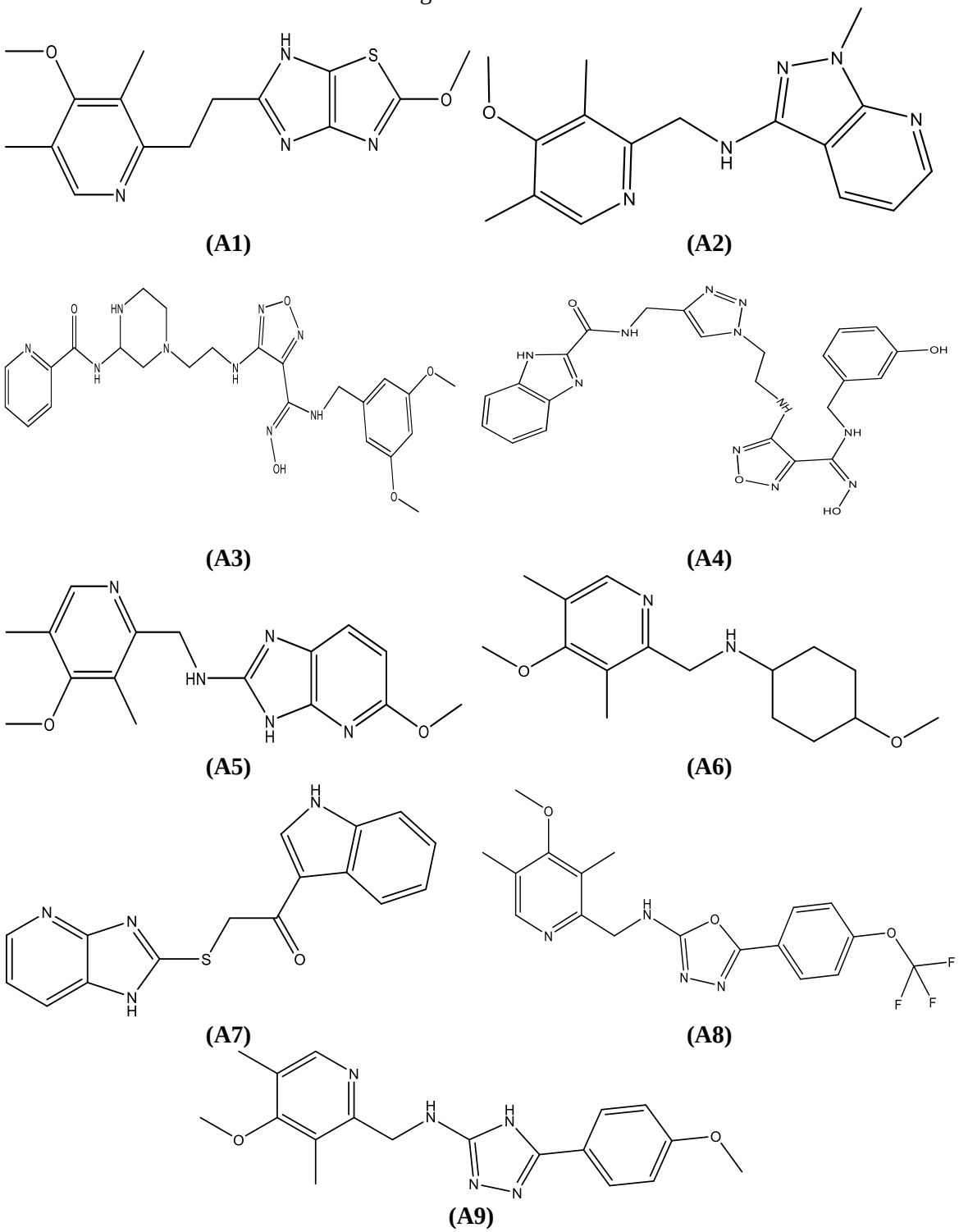


**Figure (4):** The chemical structures of finally selected hits.

### *Drug-likeness analysis*

The druggability of our finally selected candidates was assessed by calculating the ADME-T parameters; all obtained data are summarized in (Table 5). All the selected candidates revealed optimum safety, physicochemical, and pharmacokinetics profiles. So, these candidates agree with the FDA-approved conventional drugs and are highly recommended to be synthesized to test their biological activity at both *in-vitro* and *in-vivo* stages.

**Table (5):** ADME-T analysis of CPN-22 and the finally selected hits.

| | | CPN-22 | A1 | A2 | A3 | A4 | A5 | A6 | A7 | A8 | A9 | Recommender values |
|---|---|---|---|---|---|---|---|---|---|---|---|---|
| ADMET parameters | Mol_MW | 541.3 | 318.3 | 297.3 | 525.5 | 517.5 | 313.3 | 278.3 | 308.3 | 394.3 | 339.3 | 130-725 |
| | PSA | 187.0 | | | | | | | | | | 7 – 200 |
| | SASA | 758.0 | 570.8 | 575.9 | 879.9 | 892.9 | 590.9 | 566.8 | 552.7 | 642.4 | 599.5 | 300.0 – 1000.0 |
| | FOSA | 119.0 | 352.7 | 330.0 | 390.2 | 137.0 | 329.4 | 495.4 | 25.03 | 244.9 | 324.0 | 0.0 – 750.0 |
| | FISA | 265.0 | 87.26 | 41.3 | 214.1 | 357.4 | 82.1 | 16.8 | 137.3 | 61.4 | 93.9 | 7.0 – 330.0 |
| | PISA | 296.0 | 90.7 | 204.5 | 275.5 | 396.3 | 179.3 | 54.4 | 354.1 | 218.2 | 181.8 | 0.0 – 450.0 |
| | WPSA | 77.3 | 40 | 0 | 0 | 0 | 0 | 0 | 36 | 117 | 0 | 0.0 – 175.0 |
| | Volume | 1406.3 | 992 | 997 | 1579 | 1551 | 1016 | 990 | 942 | 1124 | 1066 | 500.0 – 2000.0 |
| | QPpolrz | 44.7 | 31.2 | 33.1 | 50.7 | 50.7 | 33.0 | 30.8 | 32.3 | 37.7 | 35.0 | 13.0 – 70.0 |
| | #metab⁑ | 3 | 8 | 7 | 5 | 3 | 6 | 6 | 2 | 7 | 6 | 1-8 |
| | Dipole | 12.9 | 9.40 | 4.56 | 4.68 | 8.20 | 7.17 | 2.67 | 8.10 | 7.01 | 5.23 | 1.0-12.5 |
| | QPlogPo/w | 1.5 | 3.1 | 3.7 | 0.8 | 0.6 | 3.1 | 2.8 | 3.3 | 4.6 | 3.1 | -2.0-6.5 |
| | QPlogPoct++ | 29.6 | 15.0 | 14.3 | 30.2 | 34.2 | 16.5 | 13.3 | 15.2 | 17.1 | 17.4 | 8.0-35 |
| | QPlogBB | -2.7 | -0.4 | -0.06 | -2.0 | -4.8 | -0.5 | 0.5 | -0.8 | -0.06 | -0.6 | -3 – 1.2 |
| | QPlogHERG | -6.17 | -4.5 | -5.1 | -8.4 | -7.8 | -5.1 | -4.9 | -5.7 | -5.5 | -4.9 | below –5 |
| | QPlogS | -4.0 | -4.3 | -4.5 | -2.5 | -5.0 | -4.4 | -2.8 | -4.5 | -5.9 | -4.3 | -6.0-0.5 |
| | QPlogKhsa | -0.4 | 0.1 | 0.3 | -0.4 | -0.5 | 0.2 | 0.1 | 0.3 | 0.5 | 0.2 | -1.5 – 1.5 |
| | Rule of three | 0 | 1 | 1 | 1 | 1 | 0 | 0 | 0 | 2 | 0 | <3 |
| | Rule of five | 2 | 0 | 0 | 2 | 3 | 0 | 0 | 0 | 0 | 0 | <4 |

The ADME-T properties of synthesized molecules using QiKProp module (schrödinger 12.1, LLC, NY) running in normal mode. **Mol Mw:** molecular weight of the molecule. **PSA:** van der Waals surface area of polar nitrogen, oxygen, and carbonyl carbon atoms. **SASA:** total solvent accessible surface area (SASA) in square angstroms using a probe with a 1.4 Å radius. **FOSA:** Hydrophobic component of the SASA (saturated carbon and attached hydrogen). **FISA:** Hydrophilic component of the SASA (SASA on N, O, H on heteroatoms, carbonyl C). **PISA:** π (carbon and attached hydrogen) component of the SASA. **WPSA:** Weakly polar component of the SASA (halogens, P, and S). **Volume:** Total solvent-accessible volume in cubic angstroms using a probe with a 1.4 Å radius. **QPpolrz:** Predicted polarizability in cubic angstroms. #metab⁑: number of likely metabolic reactions. **Dipole:** computed dipole moment of the molecule. **QPlogPo/w:** predicted octanol/water partition coefficient. **QPlogPoct++:** predicted octanol/gas partition coefficient. **QPlogBB:** predicted brain/blood partition coefficient. **QPlogHERG:** Predicted $IC_{50}$ value for blockage of HERG K+ channels. **QPlogS:** predicted aqueous solubility, S in mol $dm^{-3}$. **QPlogKhsa:** prediction of binding to human serum albumin. **Rule of three:** number of violations of Jorgensen's rule of 3. **Rule of five:** number of violations of Lipinski rule of 5.

## DISCUSSION

The kynurenine pathway is the main metabolic pathway responsible for metabolizing the dietary amino acid Trp. Recently it attracted the most attention and is supposed to have a key role in various pathological and pharmacological states such as cancer and rheumatoid arthritis. The two catalyzing enzymes IDO1 and TDO2 were studied exten-

sively, and many potent candidates were discovered, but unfortunately, within the clinical studies, no satisfactory results were achieved. This turned the attention to the third catalyzing enzyme (IDO2), which is currently an interesting field of research. The absence of PDB protein crystal structure, at least until now, is considered a real obstacle that led to slowing the research progress and, hence, slowing the exploration of the ambiguous pathological role of IDO2. Thus, building a proper and confident hIDO2 homology model and finding new potent and selective hIDO2 inhibitors are becoming urgent issues, our project goals here.

As a result of that shortage in libraries concerning IDO2 analog that could be applied properly, there was an obligation to build a supportive library of hits besides the found IDO library. To enhance the confident use of that library, the fragment-based drug design strategy was followed utilizing the two newly discovered promising candidates, CPN-22 and tenatoprazole. CPN-22 was selected as the most potent hIDO2 inhibitor discovered, with IC50 equaled 112 nM and selectivity index (SI=hIDO2 $_{IC50}$ / hIDO1 $_{IC50}$) equaled 4. On the other hand, however, tenatoprazole is less potent than CPN-22, with $IC_{50}$ equaled 1.5 μM, it exhibited the most SI equaled about 50. So thinking about fragmenting these two ideal candidates and trying to merge or modify the fragments that are estimated to fit and occupy the main two pockets, linker region and solvent accessible region, is supposed to get superior candidates that could be embedded more within the binding site, optimally fit the binding pockets and exhibit favored geometry. This strategy could decrease the risk of getting false ligands and be more proper for biological assays.

As a result of the absence of an hIDO2 protein crystal structure, there was an urgent to build a new hIDO2 homology model. Due to that low and problematic identity between the hIDO1 and hIDO2 (identity = 44%) to build an efficient model and get promised hits, many automated homology model servers were applied. According to the literature, it was reported that most homology models programs like Prime, SWISS-MODEL, MOE, MODELLER, ROSETTA, Composer, ORCHESTRA, and I-TASSER could produce reasonable models when the sequence identity is high. However, in the case of low sequence identity, similar to our situation here, the prime program (integrated into the maestro interface) showed better results than the other programs (55). Another advantage reported to the maestro program is utilizing the PSI-BLAST search to find the 3D- structures templates. This tool is considered a highly efficient strategy to find the best proper and accurate 3-D structures to build a high-resolution homology model (53). Then, the obtained high-ranked hIDO1 crystal structures were prepared to fix cracks and fill missing residues to be properly utilized for the building process. These prepared hIDO1 structures were subjected to prime modeling servers.

Also, aiming to improve the building process, the strategy of utilizing multiple hIDO1 templates was applied, besides using a single template, to build our homology models. As a result, the 14 newly built models were subjected to a difficult evaluation to select the best efficient, reasonable, and optimized model. The evaluating process included specific tools such as testing the amino acid superposition in 3-D structure, binding site geometry, dimension, and enveloped residues, calculating L/L and P/P RMSD, Ramachandran plot, ROC-AUC and RIE, Enrichment factor (EF), and finally evaluating the docking poses, scores, and binding affinity of positive controls. As a result, **model 4** showed the best indicators, so it was selected as a proper and reasonable model for molecular docking studies and screening.

Studying the amino acid superposing and the opposing residues between the two analogs hIDO1 and hIDO2 revealed that, however, the moderate similarity between the two paralogs hIDO1 and hIDO2, their heme-binding site implicates a high degree of amino acid conservation. As shown in (Table S1), which summarizes the residues found within the heme-binding site and entrance of hIDO1and hIDO2, replacing I-217 of hIDO1 with methionine residue in hIDO2 besides substituting of L-384 of hIDO1 with V-400 in hIDO2 inside the entrance yielded some accessibility hindrance of substrates to the binding pocket of hIDO2. These bulky residues, methionine, and valine, are also supposed to be responsible

for the differences in catalytic activity, substrate binding pattern, and the three-dimensional structures between IDO2 and IDO1(30, 56). In hIDO1, the F-227 residue plays a critical role in conserving the dioxygenase activity via involvement in substrate recognition due to its high ability to generate effective hydrophobic interactions. The Tyrosine substitutes this decisive hydrophobic amino acid in hIDO2. However, regarding the residue charge and chemical structure, this mutation from phenylalanine to Tyrosine is assumed to be conservative. However, this minimal change could manipulate the behavior of IDO2 binding pockets by reinforcing their sulfation and phosphorylation susceptibility (57). Additionally, both enzymes show differences in the position where the porphyrin-$Fe^{+2}$ structure is anchored; however, all are stabilized over the histidine residue. The heme of porphyrin is stabilized over H-346 and H-360 in hIDO1, and hIDO2, respectively, which indicates further differences in their 3-D structures and catalytic activity.

Molecular docking studies were applied to predict the interaction pattern of the ligand-protein complexes within the binding pocket. Additionally, the docking simulations were used to distinguish the promising leads by realizing the best binding poses and type of interactions observed. Docking simulation of CPN-22 and tenatoprazole to **model 4** revealed an ideal binding mode and geometry similar to that observed in the literature (35, 36). It is believed that the higher SI of tenatoprazole over CPN-22 stemmed from that better filling of pocket A. As summarized in (Table S1), replacing seven residues (especially Y-126 in hIDO1 with H-143 in hIDO2) resulted in a larger pocket A in the hIDO2 paralog. The pyridine ring structure of tenatoprazole has an ideal occupying and fitting behavior to pocket A than the Br-phenyl amide ring of CPN-22, which resulted in better SI.

On the other hand, the higher inhibition potency of CPN-22 stemmed from the better fitting of pocket B. As a result of merging and modifying those optimum fragments of both CPN-22 and tenatoprazole in a new library, new hits have been selected that are supposed to have higher potency and selectivity compared to the positive controls. The molecular docking simulation of hit **A3** shows replacing the triazole ring in CPN-22 with the piperazine ring, resulting in better binding geometry and interactions within the hIDO2 binding site. As shown in (Figure 3-E), the piperazine ring plays multi-functional roles via forming strong and short coordination bonds to the Fe+2-porphyrin structure, embedding the picolinamide amide ring more to pocket A resulted in forming better hydrophobic interaction, and the protonated nitrogen participates in further polar interactions—additionally, docking simulation of comp. **A4** (Figure 3-F) shows that replacing the Br- group in CPN-22 with the hydroxyl group created a new hydrogen bond with T-184 within pocket A. Also, replacing the pyridine ring with a benzimidazole ring resulted in forming π-cationic interaction with R-248 and a new hydrogen bond with S-252. The presence of longer linker and bulker terminals as found in compound **A7** or more lipophilic linker as found in comp. **A1** to that observed in tenatoprazole led to exhibiting better fitting and embedding character than the benzimidazole ring.

In summary, the structural activity relationship (SAR), as illustrated in (Figure 5), a 2D scheme was drawn to present the structural features preferred to achieve reasonably potent and selective IDO2 inhibitors. The SAR suggests that pocket A is optimally occupied with one Hexa-aromatic ring (blue color) and owns at least one non-protonated basic atom (X), like nitrogen. Substituting the meta or para-position with large polar functional groups like methoxy substituents is preferred to enhance the potency and selectivity. The linker (green color) is highly preferred to be simple, two carbon distance dilating from the ortho position of the ring, so the nitrogen atom will coordinate properly with the $Fe^{+2}$-porphyrin cofactor, which is a critical interaction within the binding site. As pocket B is a large and elongated structure, so could tolerate a series of aromatic and non-aromatic rings (red color) connected with 2-3 carbon chains, providing some flexibility. It is preferred to incorporate many polar functional groups, such as hydroxyl and protonated nitrogen atoms, to form hydrogen bonds with the surrounding residues. The terminal ring is preferred at meta or para positions with large polar substituents like Br or methoxy. Finally, incorporating a polar aromatic ring within the middle region

provides superior effects as it directly opposes the solvent-accessible region; this could participate mainly in stabilizing the ligand within the binding pocket and enhancing the affinity.

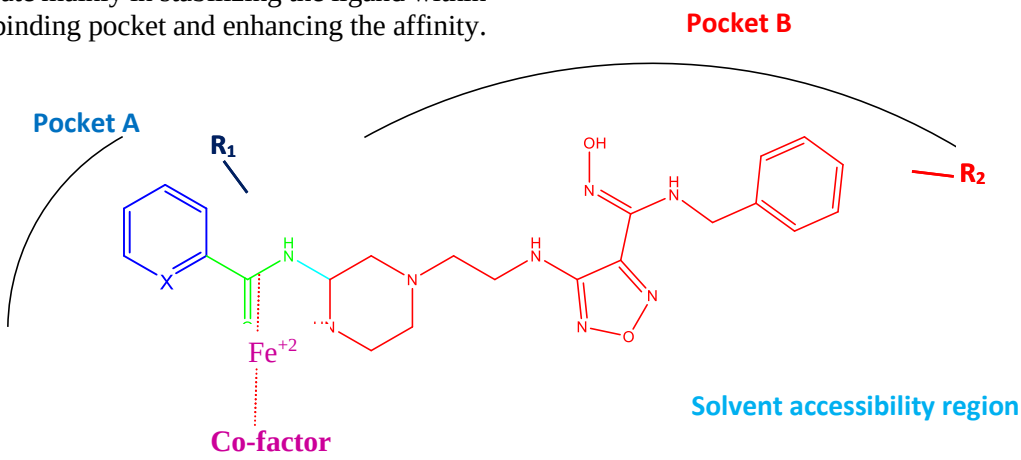


**Figure (5):** The proposed structural activity relationship (SAR) to gain potent and selective IDO2 inhibitors is shown as a 2D scheme. The X is preferred to be a non-protonated basic atom like nitrogen, while the R1 and R2 groups are supposed to be large polar functional groups at meta or para-positions.

Finally, the selected candidates showed an ideal druggability profile, and all estimated physic-chemical and pharmacokinetic descriptors locate within the recommended values and sometimes showed better druggability profiles than CPN-22.

## CONCLUSION

To sum up, the demand for new anti-cancer/anti-inflammatory drugs has become urgent. Recently, many reports indicated that the IDO2 enzyme is a key modulator and potential target in many complex diseases such as cancer and autoimmune diseases. Discovering new selective IDO2 inhibitors is still challenging due to the absence of IDO2 protein crystal structure. The rare studies on IDO2 enzymes, especially in the human type, and the few selective hIDO2 inhibitors raised the demand to find new potent and selective candidates and to examine the human type (hIDO2) more. This study described building a new hIDO2 homology model, which successfully passed all the evaluating parameters that assessed its ability to be applied confidently. To minimize the risk and to grow up the possibility of finding potent and selective candidates, two libraries of hits were utilized, the 1$^{st}$ is already found in the literature, and the 2$^{nd}$ is a self-designed library built based on the previously reported selective IDO2 and docked to our recently built homology model. As a result, 9 new candidates were discovered that are supposed to have higher potency and selectivity against hIDO2 than the reference drugs. Many strategies were applied to emphasize their activity, such as glide XP-docking score, MM-GPSA, ability to interact effectively with the $Fe^{+2}$-porphyrin, and embedded deeply within the IDO2-binding pocket. Additionally, all the selected hits showed optimum druggability and safety profiles. These newly discovered compounds are suggested to inhibit hIDO2 potentially and selectivity; they are considered promising candidates to realize the ambiguous role of IDO2 in various pathological states, particularly in cancer and rheumatoid arthritis.

### *Ethics approval and consent to participate*

Not applicable

### *Consent for publication*

Not applicable

### *Availability of data and materials*

The datasets used and/or analyzed during the current study are available from the corresponding author upon reasonable request.

### *Author's contribution*

**Mohammed T. Qaoud:** conceptualization, writing-original draft, data curation, formal analysis, methodology, resources, software, validation, visualization, and writing review & editing. **Murat Kadır Şüküroğlu:** conceptualization, funding acquisition, investigation, methodology, project administration, resources, supervision, validation, visualization, and writing review & editing.

### *Competing interests*

The authors declare that they have no competing interests.


## FUNDING

Gazi University funded this work.

## ACKNOWLEDGMENTS

The authors would like to thank Gazi University for their support.


## REFERENCES


1] Schwarcz R, Stone TW. The kynurenine pathway and the brain: challenges, controversies and promises. Neuropharmacology. 2017; 112: 237-47.

2] Lovelace M, Varney B, Sundaram G, Franco N, Ng M, Pai S. Current evidence for a role of the kynurenine pathway of tryptophan metabolism in multiple sclerosis. Front Immunol. 2016. 2016.

3] Badawy AA. Kynurenine pathway of tryptophan metabolism: regulatory and functional aspects. International Journal of Tryptophan Research. 2017; 10: 1178646917691938.

4] Wu H, Gong J, Liu Y. Indoleamine 2, 3-dioxygenase regulation of immune response. Molecular medicine reports. 2018; 17(4): 4867-73.

5] Ball HJ, Yuasa HJ, Austin CJ, Weiser S, Hunt NH. Indoleamine 2, 3-dioxygenase-2; a new enzyme in the kynurenine pathway. The international journal of biochemistry & cell biology. 2009; 41(3): 467-71.

6] Yuasa HJ, Ball HJ, Ho YF, Austin CJ, Whittington CM, Belov K, Maghzal GJ, Jermiin LS, Hunt NH. Characterization and evolution of vertebrate indoleamine 2, 3-dioxygenases: IDOs from monotremes and marsupials. Comparative biochemistry and physiology part B: biochemistry and molecular biology. 2009; 153(2): 137-44.

7] Yuasa HJ, Takubo M, Takahashi A, Hasegawa T, Noma H, Suzuki T. Evolution of vertebrate indoleamine 2, 3-dioxygenases. Journal of molecular evolution. 2007; 65(6): 705-14.

8] Jamshed L, Debnath A, Jamshed S, Wish JV, Raine JC, Tomy GT, Thomas PJ, Holloway AC. An Emerging Cross-Species Marker for Organismal Health: Tryptophan-Kynurenine Pathway. International Journal of Molecular Sciences. 2022; 23(11): 6300.

9] Chilosi M, Doglioni C, Ravaglia C, Martignoni G, Salvagno GL, Pizzolo G, Bronte V, Poletti V. Unbalanced IDO1/IDO2 Endothelial Expression and Skewed Keynurenine Pathway in the Pathogenesis of COVID-19 and Post-COVID-19 Pneumonia. Biomedicines. 2022; 10(6): 1332.

10] Britan A, Maffre V, Tone S, Drevet JR. Quantitative and spatial differences in the expression of tryptophan-metabolizing enzymes in mouse epididymis. Cell and tissue research. 2006; 324(2): 301-10.

11] Takikawa O. Biochemical and medical aspects of the indoleamine 2, 3-dioxygenase-initiated L-tryptophan metabolism. Biochemical and biophysical research communications. 2005; 338(1): 12-9.

12] Braun D, Longman RS, Albert ML. A two-step induction of indoleamine 2, 3 dioxygenase (IDO) activity during dendritic-cell maturation. Blood. 2005; 106(7): 2375-81.

13] Huang Y-S, Ogbechi J, Clanchy FI, Williams RO, Stone TW. IDO and kynurenine metabolites in peripheral and CNS disorders. Frontiers in Immunology. 2020; 11: 388.

14] Hansen A, Driussi C, Turner V, Takikawa O, Hunt N. Tissue distribution of indoleamine 2, 3-dioxygenase in normal

and malaria-infected tissue. Redox Report. 2000; 5(2-3): 112-5.

15] Wang Y, Liu H, McKenzie G, Witting PK, Stasch JP, Hahn M, Changsirivathanathamrong D, Wu BJ, Ball HJ, Thomas SR, Kapoor V. Kynurenine is an endothelium-derived relaxing factor produced during inflammation. Nature medicine. 2010; 16(3): 279-85.

16] Munn DH, Mellor AL. IDO in the tumor microenvironment: inflammation, counter-regulation, and tolerance. Trends in immunology. 2016; 37(3): 193-207.

17] Muller AJ, DuHadaway JB, Donover PS, Sutanto-Ward E, Prendergast GC. Inhibition of indoleamine 2, 3-dioxygenase, an immunoregulatory target of the cancer suppression gene Bin1, potentiates cancer chemotherapy. Nature medicine. 2005; 11(3): 312-9.

18] Lewis HC, Chinnadurai R, Bosinger SE, Galipeau J. The IDO inhibitor 1-methyl tryptophan activates the aryl hydrocarbon receptor response in mesenchymal stromal cells. Oncotarget. 2017; 8(54): 91914.

19] Liu M, Wang X, Wang L, Ma X, Gong Z, Zhang S, Li Y. Targeting the IDO1 pathway in cancer: from bench to bedside. Journal of hematology & oncology. 2018; 11(1): 1-12.

20] Alahdal M, Xing Y, Tang T, Liang J. 1-Methyl-D-tryptophan Reduces Tumor CD133+ cells, Wnt/β-catenin and NF-κβp65 while Enhances Lymphocytes NF-κβ2, STAT3, and STAT4 Pathways in Murine Pancreatic Adenocarcinoma. Scientific reports. 2018; 8(1): 1-16.

21] Ahlstedt J, Konradsson E, Ceberg C, Redebrandt HN. Increased effect of two-fraction radiotherapy in conjunction with IDO1 inhibition in experimental glioblastoma. Plos one. 2020; 15(5): e0233617.

22] Schmidt SK, Siepmann S, Kuhlmann K, Meyer HE, Metzger S, Pudelko S, Leineweber M, Däubener W. Influence of tryptophan contained in 1-Methyl-Tryptophan on antimicrobial and immunoregulatory functions of indoleamine 2, 3-dioxygenase. 2012.

23] Rich JN. Cancer stem cells in radiation resistance. Cancer research. 2007 Oct 1; 67(19): 8980-4.

24] Metz R, DuHadaway JB, Kamasani U, Laury-Kleintop L, Muller AJ, Prendergast GC. Novel tryptophan catabolic enzyme IDO2 is the preferred biochemical target of the antitumor indoleamine 2, 3-dioxygenase inhibitory compound D-1-methyl-tryptophan. Cancer research. 2007; 67(15): 7082-7.

25] Liu X, Shin N, Koblish HK, Yang G, Wang Q, Wang K, Leffet L, Hansbury MJ, Thomas B, Rupar M, Waeltz P. Selective inhibition of IDO1 effectively regulates mediators of antitumor immunity. Blood, The Journal of the American Society of Hematology. 2010; 115(17): 3520-30.

26] Long GV, Dummer R, Hamid O, Gajewski TF, Caglevic C, Dalle S, Arance A, Carlino MS, Grob JJ, Kim TM, Demidov L. Epacadostat plus pembrolizumab versus placebo plus pembrolizumab in patients with unresectable or metastatic melanoma (ECHO-301/KEYNOTE-252): a phase 3, randomised, double-blind study. The Lancet Oncology. 2019; 20(8): 1083-97.

27] Mondanelli G, Mandarano M, Belladonna ML, Suvieri C, Pelliccia C, Bellezza G, Sidoni A, Carvalho A, Grohmann U, Volpi C. Current challenges for IDO2 as target in cancer immunotherapy. Frontiers in immunology. 2021; 12: 679953.

28] Witkiewicz AK, Costantino CL, Metz R, Muller AJ, Prendergast GC, Yeo CJ, Brody JR. Genotyping and expression analysis of IDO2 in human pancreatic cancer: a novel, active target. Journal of the American College of Surgeons. 2009; 208(5): 781-7.

29] Mandarano M, Bellezza G, Belladonna ML, Vannucci J, Gili A, Ferri I, Lupi C, Ludovini V, Falabella G, Metro G, Mondanelli G. Indoleamine 2, 3-dioxygenase 2 immunohistochemical expression in resected human non-small

cell lung cancer: a potential new prognostic tool. Frontiers in immunology. 2020; 11: 839.

30] Ball HJ, Sanchez-Perez A, Weiser S, Austin CJ, Astelbauer F, Miu J, McQuillan JA, Stocker R, Jermiin LS, Hunt NH. Characterization of an indoleamine 2, 3-dioxygenase-like protein found in humans and mice. Gene. 2007; 396(1): 203-13.

31] Merlo LM, Mandik-Nayak L. IDO2: a pathogenic mediator of inflammatory autoimmunity. Clinical Medicine Insights: Pathology. 2016; 9: CPath. S39930.

32] Austin CJ, Mailu BM, Maghzal GJ, Sanchez-Perez A, Rahlfs S, Zocher K, Yuasa HJ, Arthur JW, Becker K, Stocker R, Hunt NH. Biochemical characteristics and inhibitor selectivity of mouse indoleamine 2, 3-dioxygenase-2. Amino acids. 2010; 39(2): 565-78.

33] Freewan M, Rees MD, Plaza TS, Glaros E, Lim YJ, Wang XS, Yeung AW, Witting PK, Terentis AC, Thomas SR. Human indoleamine 2, 3-dioxygenase is a catalyst of physiological heme peroxidase reactions: implications for the inhibition of dioxygenase activity by hydrogen peroxide. Journal of Biological Chemistry. 2013; 288(3): 1548-67.

34] Booth ES, Basran J, Lee M, Handa S, Raven EL. Substrate oxidation by indoleamine 2, 3-dioxygenase. Journal of Biological Chemistry. 2015; 290(52): 30924-30.

35] He G, Wan S, Wu Y, Chu Z, Shen H, Zhang S, Chen L, Bao Z, Gu S, Huang J, Huang L. Discovery of the First Selective IDO2 Inhibitor As Novel Immunotherapeutic Avenues for Rheumatoid Arthritis. Journal of Medicinal Chemistry. 2022.

36] Bakmiwewa SM, Fatokun AA, Tran A, Payne RJ, Hunt NH, Ball HJ. Identification of selective inhibitors of indoleamine 2, 3-dioxygenase 2. Bioorganic & medicinal chemistry letters. 2012; 22(24): 7641-6.

37] Koch MA, Waldmann H. Protein structure similarity clustering and natural product structure as guiding principles in drug discovery. Drug discovery today. 2005; 10(7): 471-83.

38] Paricharak S, Méndez-Lucio O, Chavan Ravindranath A, Bender A, IJzerman AP, van Westen GJ. Data-driven approaches used for compound library design, hit triage and bioactivity modeling in high-throughput screening. Briefings in bioinformatics. 2018; 19(2): 277-85.

39] Release S. 3: LigPrep; Schrödinger, LLC: New York, NY, USA, 2021. 2021.

40] Waterhouse A, Bertoni M, Bienert S, Studer G, Tauriello G, Gumienny R, Heer FT, de Beer TA, Rempfer C, Bordoli L, Lepore R. SWISS-MODEL: homology modelling of protein structures and complexes. Nucleic acids research. 2018; 46(W1): W296-W303.

41] Hildebrand A, Remmert M, Biegert A, Söding J. Fast and accurate automatic structure prediction with HHpred. Proteins: Structure, Function, and Bioinformatics. 2009; 77(S9): 128-32.

42] Impact S. LLC, New York, NY; Prime, Schrödinger, LLC, New York, NY (2021). Google Scholar There is no corresponding record for this reference.

43] Release S. 4: Schrödinger Suite 2017-4 Protein Preparation Wizard; Epik, Schrödinger, LLC, New York, NY, 2017. Impact, Schrödinger, LLC, New York, NY. 2017.

44] Kumar S, Gupta Y, Zak SE, Upadhyay C, Sharma N, Herbert AS, Durvasula R, Potemkin V, Dye JM, Kempaiah P, Rathi B. A novel compound active against SARS-CoV-2 targeting uridylate-specific endoribonuclease (NendoU/NSP15): in silico and in vitro investigations. RSC Medicinal Chemistry. 2021; 12(10): 1757-64.

45] Adasme MF, Linnemann KL, Bolz SN, Kaiser F, Salentin S, Haupt VJ, Schroeder M. PLIP 2021: expanding the scope of the protein–ligand interaction profiler to DNA and RNA. Nucleic acids research. 2021; 49(W1): W530-W4.

46] Röhrig UF, Majjigapu SR, Caldelari D, Dilek N, Reichenbach P, Ascencao K, Irving M, Coukos G, Vogel P, Zoete V, Michielin O. 1, 2, 3-Triazoles as inhibitors of indoleamine 2, 3-dioxygenase 2 (IDO2). Bioorganic & medicinal chemistry letters. 2016; 26(17): 4330-3.

47] Halgren TA, Murphy RB, Friesner RA, Beard HS, Frye LL, Pollard WT, Banks JL. Glide: a new approach for rapid, accurate docking and scoring. 2. Enrichment factors in database screening. Journal of medicinal chemistry. 2004; 47(7): 1750-9.

48] Triballeau N, Acher F, Brabet I, Pin J-P, Bertrand H-O. Virtual screening workflow development guided by the "receiver operating characteristic" curve approach. Application to high-throughput docking on metabotropic glutamate receptor subtype 4. Journal of medicinal chemistry. 2005; 48(7): 2534-47.

49] Hollingsworth SA, Karplus PA. A fresh look at the Ramachandran plot and the occurrence of standard structures in proteins. 2010.

50] Genheden S, Ryde U. The MM/PBSA and MM/GBSA methods to estimate ligand-binding affinities. Expert opinion on drug discovery. 2015; 10(5): 449-61.

51] Hawash M, Jaradat N, Abualhasan M, Qaoud MT, Joudeh Y, Jaber Z, Sawalmeh M, Zarour A, Mousa A, Arar M. Molecular docking studies and biological evaluation of isoxazole-carboxamide derivatives as COX inhibitors and antimicrobial agents. 3 Biotech. 2022; 12(12): 1-16.

52] Ioakimidis L, Thoukydidis L, Mirza A, Naeem S, Reynisson J. Benchmarking the reliability of QikProp. Correlation between experimental and predicted values. QSAR & Combinatorial Science. 2008; 27(4): 445-56.

53] Haddad Y, Adam V, Heger Z. Ten quick tips for homology modeling of high-resolution protein 3D structures. PLoS computational biology. 2020; 16(4): e1007449.

54] Palacio-Rodríguez K, Lans I, Cavasotto CN, Cossio P. Exponential consensus ranking improves the outcome in docking and receptor ensemble docking. Scientific reports. 2019; 9(1): 1-14.

55] Dolan MA, Noah JW, Hurt D. Comparison of common homology modeling algorithms: application of user-defined alignments. Homology Modeling: Springer; 2011. p. 399-414.

56] Nienhaus K, Nienhaus GU. Different mechanisms of catalytic complex formation in two L-tryptophan processing dioxygenases. Frontiers in molecular biosciences. 2018; 4:94.

57] Calalb MB, Polte TR, Hanks SK. Tyrosine phosphorylation of focal adhesion kinase at sites in the catalytic domain regulates kinase activity: a role for Src family kinases. Molecular and cellular biology. 1995; 15(2): 954-63.